



Initial concentrations of adsorbate influence on synergistic effect between a magnetic field and graphene oxide-carbon nanotube composite for Pb^{2+} and phenol adsorption

Lili Jiang^{a,*}, Haitao Yu^b, Liefei Pei^a, Wenpeng Zhang^a, Sihao Tu^a, Yimin Meng^a, Yuanshou Zhao^a, Zongshu Zou^c, Fengman Shen^c, Xingang Hou^a

^aSchool of Material Science and Technology, Lanzhou University of Technology, Langongping Road, Lanzhou 730050, Gansu Province, China, Tel./Fax: +86 931 2976378; email: jianglili2002@163.com (L. Jiang), Tel. +86 931 2976378; Fax: +86 931 2976702; email: 992632787@qq.com (L. Pei), email: zhangwp4324@163.com (W. Zhang), tushh163@163.com (S. Tu), mengyimin1993@163.com (Y. Meng), zhaoyuanshou0525@163.com (Y. Zhao), houxc1958@163.com (X. Hou)

^bDepartment of Medical Laboratory, The First Hospital of Lanzhou University, No. 1, Donggang Road, Chengguan District, Lanzhou 730000, Gansu Province, China, Tel. +86 0931 8626421; Fax: +86 0931 8619797; email: yuhaitao7707@163.com

^cSchool of Metallurgy, Northeastern University, No.3-11, Wenhua Road, Heping District, Shenyang, Liaoning Province, China, Tel./Fax: +86 24 83681545; emails: zouzs@mail.neu.edu.cn (Z. Zou), shenfmm@mail.neu.edu.cn (F. Shen)

Received 6 March 2018; Accepted 18 August 2018

ABSTRACT

The effects of initial concentrations of adsorbate on scale inhibition of circulating water and adsorption properties for Pb^{2+} and phenol were studied under the synergistic effect of the magnetic field and the adsorbent. The sulphhydryl and amino-modified graphene oxide/oxidized multiwalled carbon nanotubes (NH_2 -SH-GO/o-MWCNTs) were prepared and used as the adsorbent. The results showed that, as the initial concentration of adsorbate increased, the molecular activation energy of the circulating water also increased, while the intramolecular energy changed slightly. Meanwhile, the relative variation in the proportion of free water increased and the equilibrium adsorption capacities for Pb^{2+} and phenol also increased. The adsorption process of NH_2 -SH-GO/o-MWCNTs for Pb^{2+} and phenol under the synergistic effect of the magnetic field and the adsorbent conformed to the pseudo-second-order kinetics and Freundlich isotherm model. The aforementioned results reveal that the combined application of the magnetic field and the adsorbent can not only inhibit scale formation but also can promote the adsorption for Pb^{2+} , which showing potential for practical application.

Keywords: Graphene oxide; Multiwalled carbon nanotubes; Magnetic field; Adsorption

1. Introduction

With the continuous improvement of industrialization level, industrial wastewater has become one of the factors impeding societal development. Industrial wastewater refers to wastewater and liquid produced during industrial processes. It contains industrial production materials, intermediates, and by-products flowing as effluent with the water,

pollutants generated in production processes and water drained from production processes [1]. Industrial wastewater containing heavy metals primarily comes from mine drainage, leaching solution of waste rock piles, tailing water from concentrators, dust control water from nonferrous metal smelters, acidic cleaning wastewater from nonferrous metal processing factories and steel plants and washing water used for plated parts in electroplating factories. In addition to these, there is also industrial wastewater from electrolysis,

* Corresponding author.

and the manufacture of pesticides, medicines, paints and pigments [2,3]. Industrial wastewater mainly contains heavy metal ions such as Pb^{2+} , Zn^{2+} , Hg^{2+} , Ag^+ and Cu^{2+} [4]. Lead ion has been most frequently researched in terms of water treatment among the heavy metal ions [5]. Lead ion is ubiquitous in the environment. Human exposure can result in a wide range of biological effects, depending on the concentration and duration of exposure. Once entering the human body, lead ions can react with, and inactivate, proteins and enzymes. Once exceeding the tolerance of the human body, the person will suffer from acute, subacute or chronic poisoning, which causes damage to human health [6]. Moreover, industrial wastewater generally carries various organic substances including phenolic compounds whose excessive intake will lead to toxic symptoms such as giddiness, pruritus, anaemia and neurological disorders. In the environment, phenols are mainly generated from mining, the petrochemical industry and enterprises manufacturing polymer materials [7]. Due the enormous harm, we choose the lead ion and phenol as the object of research.

Traditional methods for dealing with industrial wastewater containing heavy metals and phenol mainly include sulphide precipitation [8], electrocatalytic oxidation [9], adsorption [10], photocatalytic oxidation [11] and membrane treatment [12]. However, these methods suffer from high cost, harsh operating conditions and unsatisfactory treatment effects. Therefore, developing an economic, environmentally-friendly, efficient treatment approach for industrial wastewater has become a research hotspot [13,14]. Adsorption is an effective method of removing pollutants from water, and its effects mainly depend on the properties of the adsorbents. The adsorbents used mainly include activated carbon, fly ash and clay. These adsorbents are limited in practical applications due to their low adsorption capacities and difficulty in regeneration [15]. Therefore, it is necessary to develop a more effective adsorption material. With a thickness of monolayer atoms, graphene oxide (GO) is a two-dimensional layered carbon nanomaterial [16], and carbon nanotubes (CNTs) are a seamless nanoscale tubular structure curled around the same central axis with a certain helical angle [17]. Both of them are nanomaterials and have high specific surface areas: this special structure endows them with many activated adsorption sites and stable chemical properties, which enable them to satisfy the basic requirements of an adsorbent [18]. By loading sulphhydryl and amino onto their surfaces, more activated adsorption sites can be formed and therefore their adsorption properties can be improved. In recent years, many scholars have prepared various GO/CNTs composite materials to treat heavy metal ions and organic pollutants in polluted water. Liu et al. [19] prepared polyacrylamide grafted graphene (PAM-g-graphene) from GO. The as-prepared PAM-g-graphene with some amino from PAM and little oxygen functional groups exhibit superior adsorption of $Pb(II)$ ions. The determined adsorption capacity of PAM-g-graphene is 819.67 mg/g (pH 6) for $Pb(II)$, which is 20 and 8 times capacities of that for graphene nanosheets and CNTs, respectively. In the previous experiment, we prepared the NH_2 -SH-GO/MWCNTs that GO and multiwalled carbon nanotubes (MWCNTs) were chemically modified with amino and sulphhydryl groups for simultaneous

adsorption of pollutants, such as Pb^{2+} , Zn^{2+} and phenol in water solution. The maximum adsorption capacity of NH_2 -SH-GO/MWCNTs was 125.8, 98.6 and 23.8 mg/g for Pb^{2+} , Zn^{2+} and phenol, respectively [20]. Alijani et al. [21] prepared a CNT composite material with natural magnetism and studied its adsorption properties for mercury. They concluded that the composite material has superparamagnetism and its maximum adsorption capacity for mercury was as high as 200 mg/g, with a removal rate of 99.1%. Haibo Wang et al. [22] report a large-scale and low-cost approach for the synthesis of three-dimensional (3D) polyvinyl alcohol/CNTs nanoporous architecture using self-assembly method. An outstanding adsorption of 225.6 mg/g for $Ni(II)$ ions was achieved for 3D nanoporous structure, which was 18-fold more than that for CNT powders and much higher than that for other sorbents reported in literature.

In addition, scale can bring serious problems for the circulating water system. But the conventional chemical method for treatment scale is high costs and high energy consumption. Magnetic field treatment, however, is a very promising method of scale prevention which integrates various functions including scale prevention and removal. Heavy metal ion pollution and scale will occur simultaneously in industrial water circulation. But there is no way to solve the problem of heavy metal and scale pollution at the same time. At present, only one kind of pollution problem is solved alone. So in order to solve the problem of heavy metal ions and the scale pollution at the same time, this project proposes a new kind of method: the synergy of magnetic field and new adsorbent can solve the heavy metal ions pollution and the scale in the circulation water. To the author's knowledge, the synergistic effect between magnetic field and adsorbent has been not researched.

The research aims to explore the effects of initial concentration of adsorbates on the scaling inhibition of circulating water and the adsorption capacity under the synergistic effect between the magnetic field and the adsorbent. Here, the adsorbent was a prepared sulphhydryl- and amino-modified GO/oxidized multiwalled CNTs (NH_2 -SH-GO/o-MWCNT). Analyses of the reaction kinetics and adsorption isotherms were also discussed. Moreover, variation of molecular activation energy and relative variation in the proportion of free water also are discussed to research the effects of magnetic field on scale inhibition.

2. Experiment and methods

2.1. Materials and reagents

MWCNTs were purchased from Shenzhen Nanotech. Port Co. Ltd, (China). According to the manufacturer, the diameters of the MWCNTs are in the range from 20 to 30 nm and their specific surface areas range from 100 to 160 m²/g. Ultrapure water was used for solution preparation. Lead nitrate and phenol were purchased from Tianjin Fu Rui Technology Co. Ltd (China). Nitric acid, sulphuric acid, hydrazine and acetone (purity > 99.5%) were purchased from Big Alum Chemical Reagent Factory (China). The (3-mercaptopropyl)trimethoxysilane (MPTS) was purchased from Beijing Biological Technology (China). All of the

chemicals were of analytical grade and used without further purification.

2.2. Characterization techniques

A transmission electron microscope (TEM) (type JEM-2010, operating at 200 kV) was used to analyse the morphology of the samples. Fourier-transform infrared (FT-IR) spectra were recorded using a Nexus-870. All of the samples were prepared by mixing KBr with the modified MWCNTs and spectra recorded over the range 400–4,000 cm^{-1} . The concentration of lead ions was determined using a Hitachi Z-5000 atomic absorption spectrophotometer, and that of phenol was measured using an ultraviolet-visible spectrophotometer (model VU-1000). All of the water used in these experiments was produced using an ultrapure water system (Ulupure, UPD-I-20T). Fig. 1 showed the devices used to investigate the synergistic effect.

2.3. Preparation of $\text{NH}_2\text{-SH-GO/o-MWCNTs}$

0.1 g of GO and 0.2 g of o-MWCNTs were dispersed in 100 mL of absolute alcohol, respectively. Then the dispersion liquids were treated for 2 h with ultrasound. Mixed the above solution, placed into a three-necked bottle and treated the mixture with ultrasound for another 2 h. Finally, filtered and washed with deionized water for several times. Put the mixtures in a vacuum oven for 12 h at 80°C. The obtained product is the GO/o-MWCNTs used in the next stage. A portion of the GO/o-MWCNTs (200 mg) was added to 40 mL of absolute alcohol at 25°C. Then, 4 mL of acetic acid and 8 mL of MPTS were added in the above mixtures and the solution left for 24 h. 100 mL of acetone was slowly dispersed into the solution. The SH-GO/o-MWCNTs were filtered and washed several times with ultrapure water. A sample of the SH-GO/o-MWCNTs (100 mg) was dispersed in 50 mL of absolute alcohol. The mixture was stirred vigorously and 10 mL of hydrazine hydrate was added. Then, the mixture was further stirred for 6 h. Subsequently, the composite was filtered and washed with deionized water. Finally, the product was dried in a vacuum oven at 80°C for 8 h. The product finally obtained was the $\text{NH}_2\text{-SH-GO/o-MWCNTs}$.

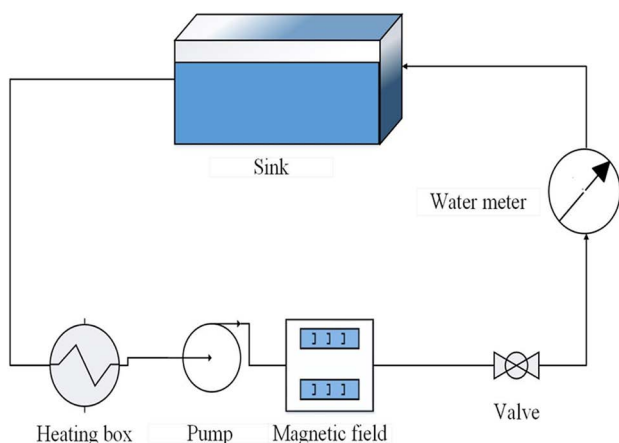


Fig. 1. The devices used to investigate the synergistic effect between a magnetic field and $\text{NH}_2\text{-SH-GO/o-MWCNTs}$.

2.4. Influence of initial concentrations of adsorbates on scale inhibition performance and adsorption

The technician first added 10 L of configured solutions into the circulating water system. The configured solution containing Ca^{2+} , Pb^{2+} and phenol at initial concentrations of 30, 50, 70 and 90 mg/L was separately prepared. Adjusted the flow velocity (0.17 m/s), magnetic field intensity (0.54 T) and temperature (30°C). The previous experimental result revealed that there was an optimal scale-inhibition effect under these experimental conditions. The magnetic treatment and adsorption experiment were conducted after starting the circulating water system where the $\text{NH}_2\text{-SH-GO/o-MWCNTs}$ with an initial concentration of 50 mg/L (prepared in advance) was added. Afterwards, the pH, conductivity, viscosity and surface tension at 5, 15, 25, 35, 45, 60, 75, 100, 140, 195, 285, 405, 525 and 685 min were measured. On this basis, relative variations in intramolecular energy and molecular activation energy were calculated. Additionally, small water specimens with different initial concentrations were extracted separately at 0 and 685 min to measure the peak width at half height of the circulating water by using a nuclear magnetic resonance (NMR) spectrometer. By doing so, the variation of the proportion of free water molecules in circulating water was further calculated. The concentrations of Pb^{2+} and phenol were measured separately by atomic absorption spectrophotometry and an ultraviolet-visible spectrophotometer. On this basis, the adsorption quantities of the adsorbent for lead ions and phenol were calculated. The adsorption capacity (q_t) of the adsorbent can be calculated using the following formula (1) [23]:

$$q_t = \frac{(C_0 - C_e)V}{m} \quad (1)$$

where q_t is the quantity adsorbed at time t by the adsorbent (mg/g); C_0 and C_e are the initial and equilibrium concentrations of adsorbate (mg/L), respectively; V is the volume of the solution (L), and M is the mass of adsorbent (g). The experimental data for adsorbing Pb^{2+} and phenol were fitted by using pseudo-first-order and second-order kinetic models. The pseudo-first-order kinetic equation can be expressed as follows [24]:

$$\ln(q_e - q_t) = \ln q_e - k_1 t \quad (2)$$

where q_e and q_t refer to the adsorption capacities (mg/g) of the adsorbents at equilibrium and at time t , respectively. Moreover, k_1 and t represent the rate constant (min^{-1}) of the pseudo-first-order kinetic equation and time (min), respectively. According to the pseudo-first-order kinetic equation, a graph was drawn for t by using $\ln(q_e - q_t)$ and the slope of the resulting line was the rate constant k_1 . The pseudo-second-order kinetic equation is given by Eq. (3) [25]:

$$\frac{t}{q_t} = \frac{1}{k_2 q_e^2} + \frac{t}{q_e} \quad (3)$$

where k_2 refers to the rate constant (g/mg/min) of the pseudo-second-order kinetic equation. The values of t/q_t were plotted against t and then the values of parameters q_e and k_2 can be

calculated by using the slope and intercept of the obtained straight line.

The Langmuir isotherm model is given by Eq. (4) [26]:

$$\frac{1}{q_e} = \frac{1}{bq_m C_e} + \frac{1}{q_m} \quad (4)$$

where C_e and q_e refer to the concentration (mg/L) of target in the circulating water and equilibrium adsorption capacity (mg/g) of the adsorbent under adsorption equilibrium, respectively. Moreover, q_m and b represent the maximum adsorption capacity (mg/g) and adsorption constant (L/mg), respectively. The graph of $1/C_e$ was drawn by using $1/q_e$ and then the adsorption constant b and parameter q_m can be acquired according to the slope and intercept of obtained straight line.

The Freundlich isotherm model assumes that the adsorption process occurs on the surface of an inhomogeneous medium, which has multilayer adsorption capabilities owing to the different adsorption sites having different binding energies and affinities. The Freundlich isotherm model is given by Eq. (5) [27]:

$$\ln q_e = \ln k_f + \frac{1}{n} \ln C_e \quad (5)$$

where q_e and C_e represent the adsorption capacity (mg/g) of the adsorbent and the concentration of adsorbates (mg/L) under adsorption equilibrium conditions, respectively. Moreover, k_f and n refer to constants separately related to adsorption capacity and adsorption strength.

The relative variation in the proportion of free water molecules depends on the quantities of hydrogen bonds in the circulating water, which can be measured by using the peak width at half height from NMR spectrometric data, calculated as follows [28]:

$$\frac{\Delta C}{C_0} = \frac{C - C_0}{C_0} = \frac{\Delta v_{1/2}^0 - \Delta v_{1/2}}{\Delta v_{1/2}} \quad (6)$$

where C is the proportion of free water after magnetic treatment, C_0 is the proportion of free water without magnetic field and $\Delta C/C_0$ is the relative variation in the proportion of free water. In addition, $\Delta v_{1/2}$ is the experimental peak width at half height under magnetic field and $\Delta v_{1/2}^0$ the initial peak width at half height without magnetic field.

The relative variation of intramolecular energy mainly depends on the surface tension, calculated as follows [29]:

$$\frac{E^{\text{Inner}} - E_0^{\text{Inner}}}{E_0^{\text{Inner}}} = \frac{\Delta E}{E_0} = \frac{S - S_0}{S_0} = \frac{T - T_0}{T_0} \quad (7)$$

where E^{Inner} refers to the intramolecular energy (J), S to entropy (J/mol/K) and T to surface tension (N/m). As before, a subscript '0' refers to an initial value (before application of the magnetic field) and unsubscripted values to those after magnetic treatment. Thus, $(E^{\text{Inner}} - E_0^{\text{Inner}})/E_0^{\text{Inner}}$ represents the relative change in intramolecular energy caused by the magnetic field.

The variation of activation energy is determined according to the viscosity, calculated as follows [30]:

$$\Delta E' = -RT \ln \left(\frac{\eta}{\eta_0} \right) = E' - E'_0 \quad (8)$$

where $\Delta E'$ refers to the variation of activation energy; E' and E'_0 represent the molar activation energies (J/mol) of experimental and control (ultrapure water) groups, respectively; R represents gas constant (J/(mol K)) and T means temperature (K). Additionally, η and η_0 refer to the viscosities of the experimental and control groups, respectively.

3. Results and discussion

3.1. TEM

Fig. 2 shows TEM images of primary MWCNTs, purified MWCNTs, GO/o-MWCNTs and $\text{NH}_2\text{-SH-GO/o-MWCNTs}$. Fig. 2(a) shows that the primary MWCNTs have tubular structures and smooth tubular walls of 20–30 nm in diameter, as well as apparent agglomerations, which are consistent with the tube diameters set by manufacturers. There were many residual catalyst impurities on the surface of the tube walls. To improve the adsorption capacity of MWCNTs, it is necessary to purify the MWCNTs. Fig. 2(b) shows the purified MWCNTs: the surface of the MWCNTs was coarse and, the dispersion significantly improved without residual catalyst impurities being found; surface features measuring about 30–40 nm in diameter were also seen. The MWCNTs were corroded by strong acids and subjected to fracturing, which resulted in their reduced length, further causing an increase in specific surface area and in the number of surface adsorption sites so as to improve the adsorption capacity of MWCNTs. The interfaces of MWCNTs were opened, which provided adsorption sites for oxygen-containing functional groups (such as carboxyl and hydroxyl). Fig. 2(c) showed that GO had a lamellar structure and the layers were closely combined with each other, measuring about 1,200–1,500 nm wide and exhibiting a thin structure with numerous folds. The gap among GO layers increased due to oxidation. Fig. 2(d) shows that thin GOs were interlaced with MWCNTs of about 30–40 nm in diameter. MWCNTs adsorbed onto the surface of GO, which directly indicated the successful preparation of $\text{NH}_2\text{-SH-GO/o-MWCNTs}$.

3.2. FT-IR

Fig. 3 shows FT-IR spectra of GO/o-MWCNTs and $\text{NH}_2\text{-SH-GO/o-MWCNTs}$. Fig. 3(a) shows that a strong peak appeared at $1,620 \text{ cm}^{-1}$ in the FT-IR spectrum of GO/o-MWCNTs and was a stretching vibration peak of C=C, implying that the sp^2 structure of graphite was undamaged. Fig. 3(b) shows that the basic structure of graphite was still undamaged despite being modified by amino and sulphhydryl groups. Additionally, the strong peaks at $3,450$ and $1,725 \text{ cm}^{-1}$ separately belonged to the stretching vibration peaks of C–O and C=O. They appeared because large amounts of hydroxyl and carboxyl groups were introduced during the oxidation of graphite and the purification of the MWCNTs [31]. Compared with the FT-IR spectrum of

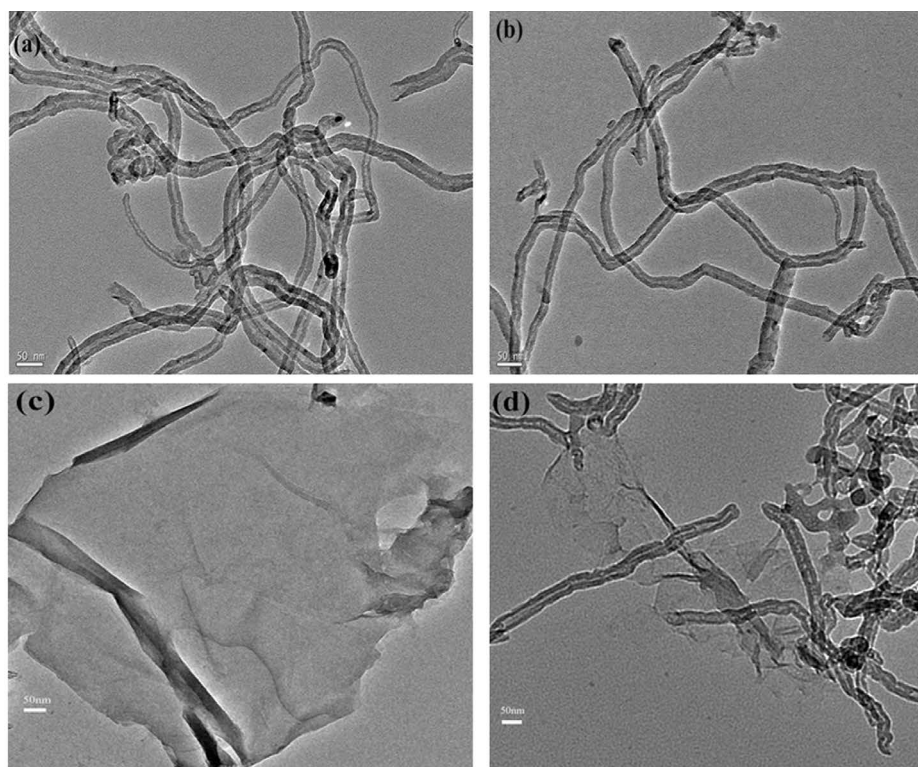


Fig. 2. TEM images of carbon nanotubes, (a) original MWCNTs, (b) purified MWCNTs, (c) GO, and (d) $\text{NH}_2\text{-SH-GO/o-MWCNTs}$.

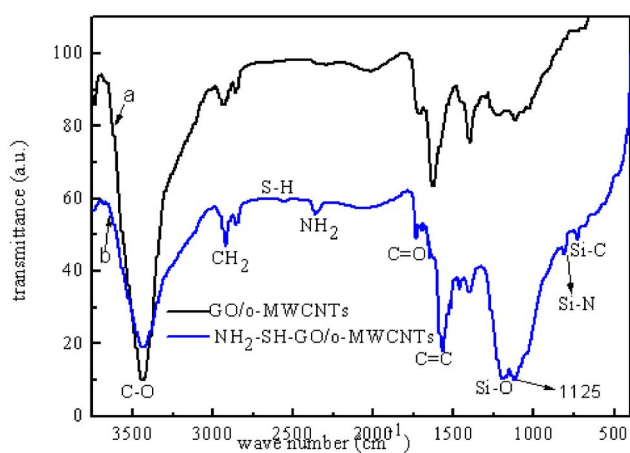


Fig. 3. FT-IR spectra of (a) GO/o-MWCNTs and (b) $\text{NH}_2\text{-SH-GO/o-MWCNTs}$.

GO/o-MWCNTs, the intensity of the C=O peak in the $\text{NH}_2\text{-SH-GO/o-MWCNTs}$ decreased and this was mainly because a part of the C=O groups were reduced by hydrazine hydrate during the addition of the groups, thus weakening the peak. Additionally, the spectrum of $\text{NH}_2\text{-SH-GO/o-MWCNTs}$ shows that new absorption peaks occurred at 1,245, 720 and 750 cm^{-1} , which are the stretching vibration peaks of Si-O, Si-C and Si-N, respectively [32]. The result indicated that MPTS had been loaded onto the surface of MWCNTs or GO, being connected with oxygen-containing groups in graphite and MWCNTs, and amino was also connected with MPTS.

The absorption peak at 2,360 cm^{-1} was the stretching vibration peak of -NH_2 , indicating that there were amino groups in the $\text{NH}_2\text{-SH-GO/o-MWCNTs}$. There was a weak absorption peak at 2,560 cm^{-1} , which was the stretching vibration peak of S-H. Moreover, the band from 2,800 to 3,000 cm^{-1} belonged to the stretching vibration of -CH_2 and had a greater intensity than the peaks of the GO-MWCNTs without being modified by other groups. This was mainly caused by the -CH_2 groups on MPTS. These results implied that MPTS were connected with GO/MWCNTs while sulphhydryl and amino groups were also loaded on the surface of the GO/MWCNTs.

3.3. Influence of initial concentration on scale inhibition performance and adsorption

3.3.1. Influence of initial concentration on pH value and conductivity

Fig. 4 shows the changes in pH value and conductivity under different initial concentrations of adsorbates. The experimental conditions were as follows: flow velocity (0.17 m/s), magnetic field intensity (0.54 T), temperature (30°C) and concentration of adsorbent (50 mg/L). It can be seen from Fig. 4(a) that the pH value of the circulating water with an initial concentration of 30 mg/L gradually decreased and remained stable after 75 min with increasing magnetic treatment time. The primary reason was that the circulating water was an open system and CO_2 in air was constantly dissolving in the circulating water to form carbonic acids. After primary and secondary ionisation, carbonic acids produced sufficient hydrogen ions in circulating water to cause the pH of the circulating water to decrease. When the Ca^{2+} , Pb^{2+} and

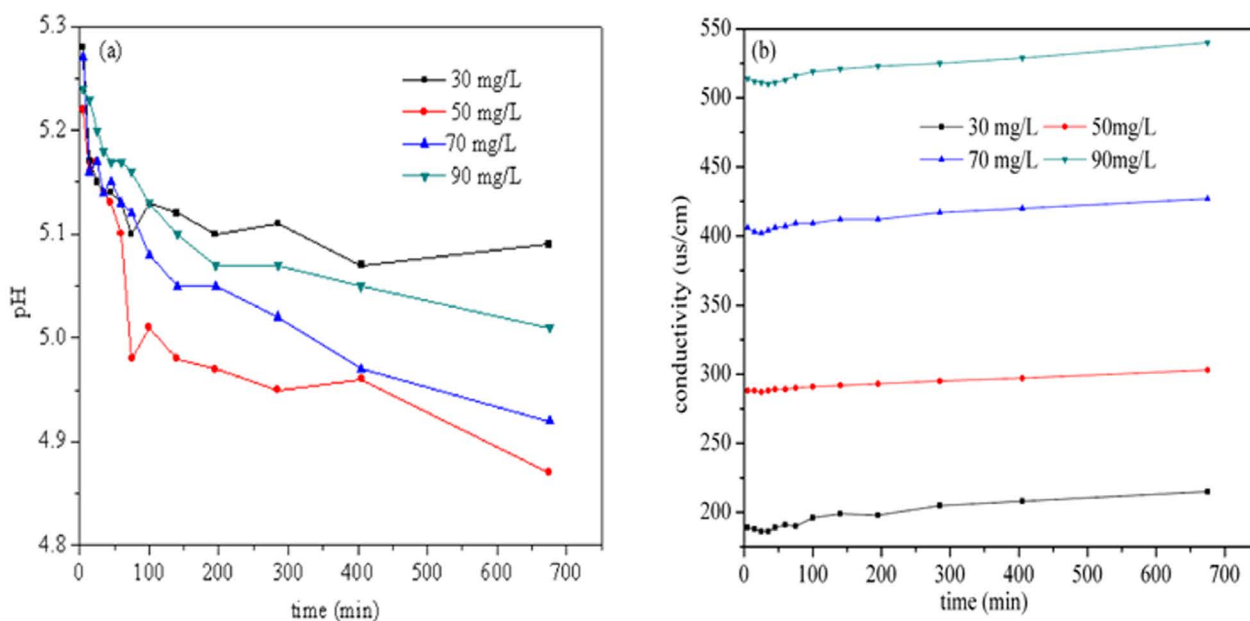


Fig. 4. Influence of initial concentration on pH (a) and conductivity (b).

phenol, with initial concentrations of 50 mg/L, were added to the circulating water, the pH decreased at first and then remained stable. The pH value under the initial concentration of 50 mg/L decreased more significantly compared with that under the initial concentration of 30 mg/L, implying that sufficient hydrogen ions were generated in the circulating water. Additionally, the decrease of pH was also related to that the reaction between calcium ions and ionized bicarbonate ions released by the abundant hydrogen ions. The combined effect of these two aspects rapidly decreased the pH of the circulating water. As observed from the changes in conductivity (Fig. 4(b)), the conductivity remained unchanged at different initial concentrations over increasing magnetic treatment time. This indicated that the circulating water basically remained unchanged with regard to its conductivity and water quality was extremely stable. Serious scale-forming phenomenon did not occur, implying that a magnetic field can inhibit the production of scale. However, the higher the initial concentration is, the higher the conductivity is. The conductivity of the circulating water at an initial concentration of 90 mg/L was far higher than that of the circulating water at an initial concentration of 30 mg/L. The higher the ion concentration added to the circulating water, the more numerous the conductive ions are, and therefore the higher the conductivity is.

3.3.2. Influence of initial concentrations on variation of activation energies and relative variation of intramolecular energies

Fig. 5 shows the changes in variation of activation energies and relative variation of molecular internal energies in the circulating water under different initial concentrations. It can be seen from Fig. 5(a) that the viscosity of circulating water at a concentration of 30 mg/L first increased and then stabilized with increasing magnetic treatment time, implying

that the force among water molecules in the circulating water increased. With increasing concentration, the same behaviour continued. It can be seen, from the surface tension data, that the surface tension of the circulating water gradually decreased with increasing magnetic treatment time and the decreasing trend continued with rising concentration (Fig. 5(b)). It can be clearly observed from Fig. 5(c) that variation of molecular activation energies increased overtime. Compared with that circulating water without magnetic treatment, the activation energies of circulating water undergoing magnetic treatment gradually increased as well as the energy required for circulating water to be transformed from a stable to an active state. The molecular activation energy first increased and then stabilized after the circulating water with magnetic treatment at magnetic field intensity of 0.54 T. The variation of molecular activation energy of the circulating water at an initial concentration of 30 mg/L reached 1.1 J/mol at 400 min (magnetic treatment time). This implied that molecular activation energy increased significantly and the circulating water reached a stable state wherein further chemical reactions, namely, the production of calcium carbonate, were difficult. As the initial concentration further increased, the change in molecular activation energies became more significant. These results revealed that magnetic field can inhibit the formation of scale. Fig. 5(d) shows that the intramolecular energies of circulating water undergoing magnetic treatment decreased with increasing magnetic treatment time. Moreover, with increasing initial concentrations, the relative variation of molecular internal energies constantly decreased within the range 0.05%–0.1%. The result indicated that initial concentrations exerted an insignificant influence on the intramolecular energies. The relative variation of intramolecular energies was negative, which suggested that the intramolecular energy of the circulating water was far lower than that in the ultrapure water. The reduction of intramolecular energies implied that circulating water changed to a stable state and

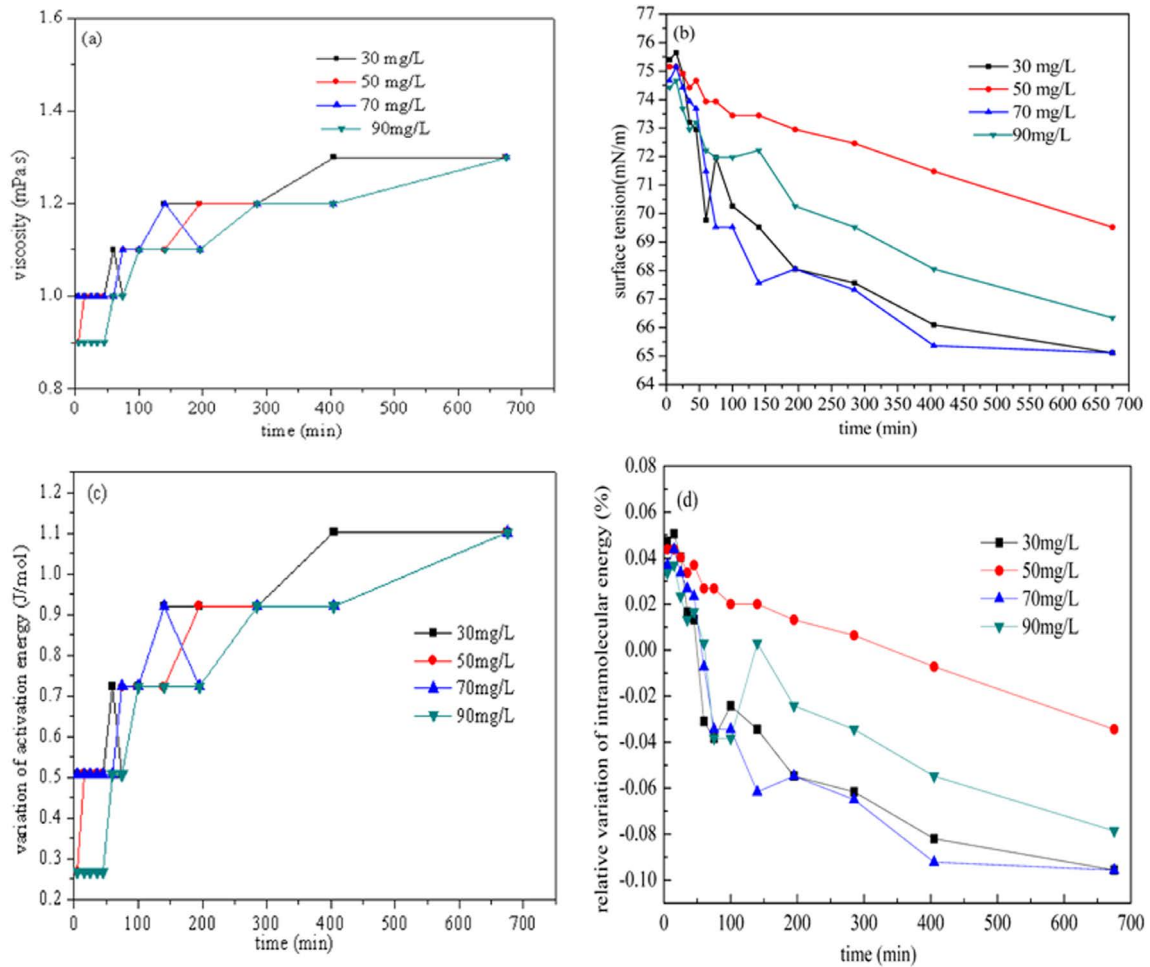


Fig. 5. Influence of initial concentration on viscosity(a), surface tension(b) variation of activation energy (c) (3) and relative variation of intramolecular energy (4).

calcium ions were unlikely to react with carbonate ions in the circulating water, thus giving rise to the desired scale-inhibitory effect [33].

3.3.3. Influence of initial concentrations on relative variation of proportion of free water

Fig. 6 shows the relative variation of proportion of free water under different initial concentrations and magnetic field intensities: as the initial concentrations of target ions increased, the relative variation of proportion of free water in the circulating water without magnetic treatment fluctuated within the range of 5.02% and 13.43%. The negative relative variation indicated that the proportion of free water molecules decreased. The water molecules mainly appear as free water molecules and bound water. The free water molecules are far from the bound water layer and the thermodynamic equilibrium relationships are fluctuant between free water molecules and bound water. The structure of water molecules changed with the formation or damage of hydrogen bonds. When the magnetic field intensity was 0.27 T, the higher the initial concentrations of Pb^{2+} and phenol were, the lower relative variation of proportion of free water within the range from 9.23% to 21.15%. The proportion of free water molecules

in the circulating water decreased while that of the bound water molecules increased. More water molecules appeared as hydrated ions, so that more calcium and carbonate ions can be combined with water molecules. Owing to calcium

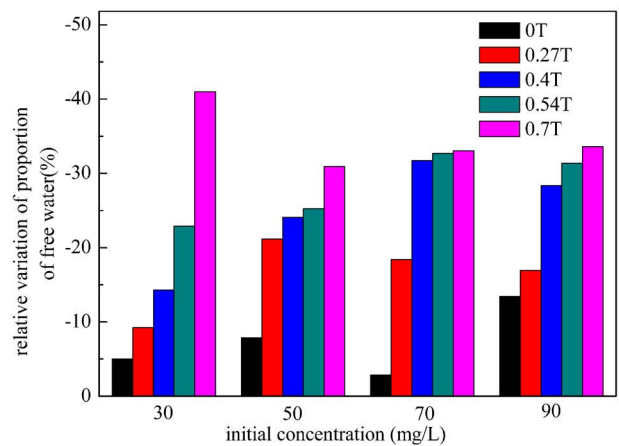


Fig. 6. The influence of initial concentration on the relative variation of proportion of free water.

and carbonate ions being bound near the clusters of water molecules, the probability that calcium ions reacted with carbonate ions decreased, which was conducive to inhibiting scale-formation. The result also indicated that the increase in initial concentrations was conducive to the formation of hydrogen bonds and strengthening the degree of association between water molecules. The relative variation of proportion of free water was significantly reduced with increasing magnetic field intensities. It indicated that the proportion of free water molecules in the circulating water undergoing magnetic treatment declined while that of bound water rose, which was favourable for inhibiting scale-formation.

3.3.4. Influence of initial concentrations on adsorption capacities

3.3.4.1. Influence of adsorption time and adsorption kinetics

Adsorption time is an important parameter influencing the adsorption effect under the synergistic effect of a magnetic field and $\text{NH}_2\text{-SH-GO/o-MWCNTs}$ and therefore a kinetic analysis of the adsorption effect is undertaken. Fig. 7 shows the changes in adsorption capacities under different initial concentrations. As shown in Fig. 7(a), the adsorption capacity for lead ions rapidly increased at first and then tended to stabilize with increasing magnetic treatment time at a magnetic field intensity of 0.54 T and initial concentration of 30 mg/L. The adsorption capacity of the adsorbent for Pb^{2+} was 117.54 mg/g after 45 min. The adsorption capacities of $\text{NH}_2\text{-SH-GO/o-MWCNTs}$ are four and two times as strong as that of graphene nanosheets and magnetic chitosan/GO, respectively [34–35]. And the process time of adsorption achieved equilibrium for their samples was 24 h, which was much longer than our report in the work (45 min). The earlier results illustrated the excellent adsorption performance of the prepared adsorbent. This was mainly because plenty of groups (amino, sulphhydryl, carboxyl and hydroxyl) appeared on the surface and edge of the $\text{NH}_2\text{-SH-GO/o-MWCNTs}$. The

groups can be combined with water molecules and adsorbates to form a spatial network structure under the effect of hydrogen bonds and Van der Waals (VDW) force to improve the adsorption capacity of the adsorbent. Additionally, the adsorbent exhibited a large specific surface area and contained many porous structures, which were conducive to increasing the adsorption capacity of the adsorbent. With increasing initial concentrations, the adsorption capacity for lead ions increased and the equilibrium adsorption capacity was far larger than the adsorption capacity under the initial concentration of 30 mg/L. The result indicated that the higher the initial concentration, the larger the adsorption capacity of the adsorbent for lead ions. Therefore the higher the concentrations of adsorbates are in water, the larger concentration difference between solid and liquid. And the larger the driving force that adsorbates move to adsorbent surface is. Therefore, the adsorption capacity of the adsorbent was greater than that in the circulating water with an initial concentration of 30 mg/L.

Fig. 7(b) shows the changes of adsorption capacities for phenol under the synergistic effect of the magnetic field and $\text{NH}_2\text{-SH-GO/o-MWCNTs}$. At the initial concentration of 30 mg/L, the adsorption capacity rapidly increased at first and then stabilized overtime: the equilibrium adsorption capacity was 24.79 mg/g. With increasing initial concentrations, the equilibrium adsorption capacity of $\text{NH}_2\text{-SH-GO/o-MWCNTs}$ for phenol also increased. The equilibrium adsorption capacities of the adsorbent for phenol at initial concentrations of 50, 70 and 90 mg/L were 29.68, 44.35 and 50.47 mg/g, respectively.

The adsorption processes with different initial concentrations were fitted by using Lagrange pseudo-first and second-order kinetic equations and the fitting result using pseudo-second-order kinetics is shown in Fig. 8. The parameters are displayed in Table 1. The adsorption capacity $q_{\text{ca,e}}$ was calculated according to the slope of the fitted straight line in Fig. 8 and the adsorption rate constant k_2 was obtained

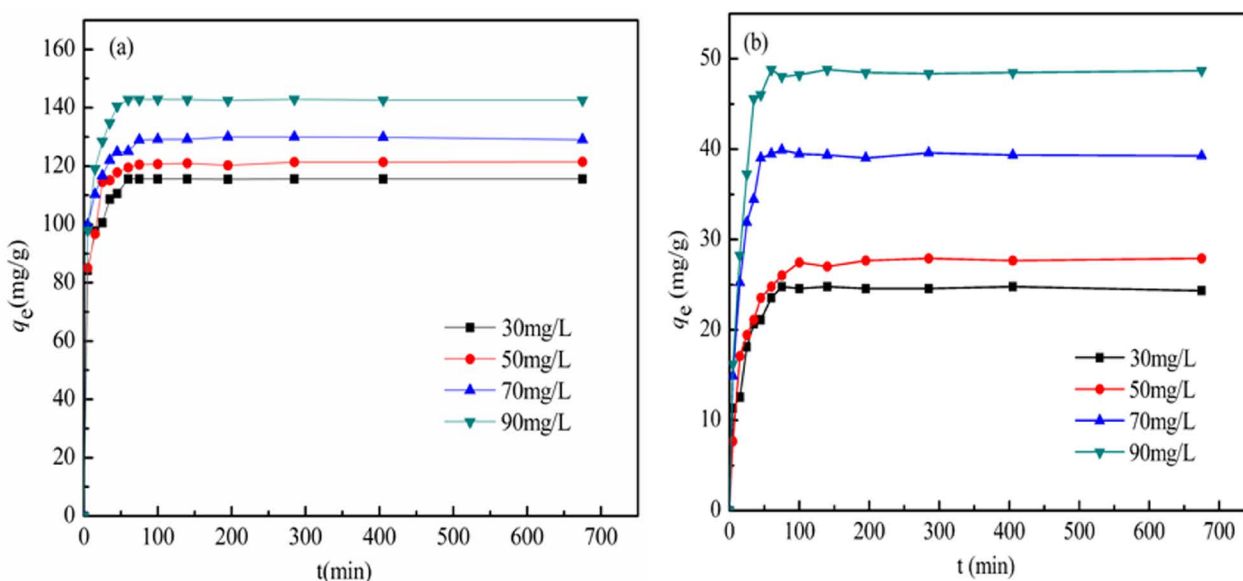


Fig. 7. Influence of initial concentrations on adsorption capacity, (a) Pb^{2+} , and (b) phenol.

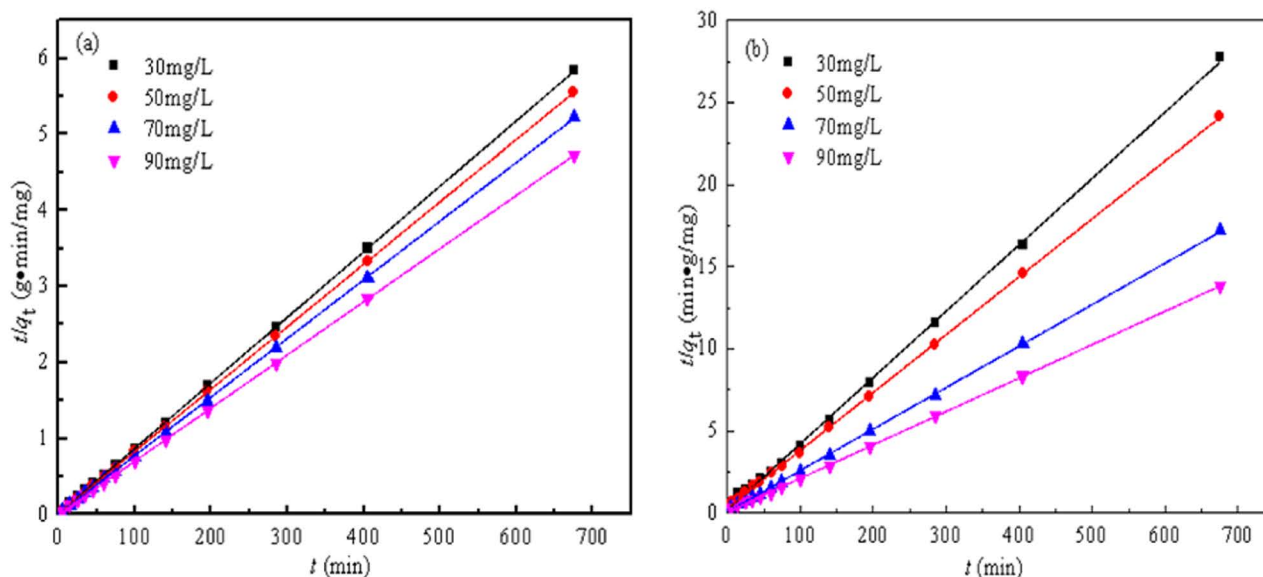


Fig. 8. Pseudo-second-order kinetics model for (a) Pb^{2+} , and phenol (b).

Table 1
Fitted adsorption kinetic results for different initial concentrations

Adsorbate	Concentration (mg/L)	Pseudo-first-order model			Pseudo-second-order model				
		$q_{ca,e}$ (mg/g)	k_1 (min^{-1})	R^2	$q_{ex,e}$ (mg/g)	$q_{ca,e}$ (mg/g)	h (mg/g/min)	k_2 (g/mg)	R^2
Pb^{2+}	30	0.97	0.00833	0.486	115.63	116.01	74.02	0.0055	0.999
	50	6.35	0.00972	0.884	120.90	121.95	68.41	0.0046	0.999
	70	4.49	0.00654	0.588	129.99	129.70	95.89	0.0057	0.999
	90	17.88	0.00139	0.477	142.85	143.06	110.52	0.0054	0.999
Phenol	30	1.31	0.00553	0.427	24.81	24.76	5.09	0.0083	0.999
	50	5.59	0.01121	0.858	27.91	28.38	3.22	0.0040	0.999
	70	1.57	0.00439	0.436	39.64	39.62	11.93	0.0076	0.999
	90	2.80	0.00518	0.534	48.92	49.14	10.87	0.0045	0.999

based on the intercept of the fitting straight line. The values are listed in Table 1: the adsorption processes of $\text{NH}_2\text{-SH-GO/o-MWCNTs}$ for Pb^{2+} and phenol conformed to the pseudo-second-order kinetic model ($R^2 = 0.999$), implying that the adsorption rate was directly proportional to the concentrations of the two adsorbates. Additionally, the equilibrium adsorption capacities obtained based on pseudo-second-order kinetic model were all close to the experimental values, indicating the accuracy of fitting results. With increasing initial concentration, the equilibrium adsorption capacities of $\text{NH}_2\text{-SH-GO/o-MWCNTs}$ for Pb^{2+} and phenol gradually increased, which was consistent with the results shown in Fig. 7. As shown in Table 1, the adsorption rate constant k_2 for lead ions was close to that for phenol, which indicated that the adsorption rate of the adsorbent for Pb^{2+} was the same as that for phenol. With increasing initial concentration, the adsorption rate constant for lead ions remained unchanged, implying that concentration exerted an insignificant influence on the adsorption rate for lead ions. However, the adsorption rate constant for phenol gradually decreased with

rising initial concentration, which indicated that the higher the initial concentration of phenol, the lower the adsorption rate constant. This was probably because there was a strong competitive relationship between phenol and Pb^{2+} during the adsorption process.

3.3.4.2. Adsorption isotherms

Adsorption isotherm analysis is a typical method used to analyse adsorption data and exploring the underpinning mechanisms. Langmuir and Freundlich isotherm models are generally used to investigate the adsorption mechanism. The Langmuir model is mainly used to describe uniform, monolayer adsorption, namely, it is assumed that all adsorption sites on the surface of an adsorbent have the same attractive forces for adsorbates. By contrast, it is supposed that an adsorption process is nonuniform and undergoes multilayer adsorption in the Freundlich isotherm model. The adsorption process was fitted by Langmuir and Freundlich isotherm models and the fitting result using the Freundlich

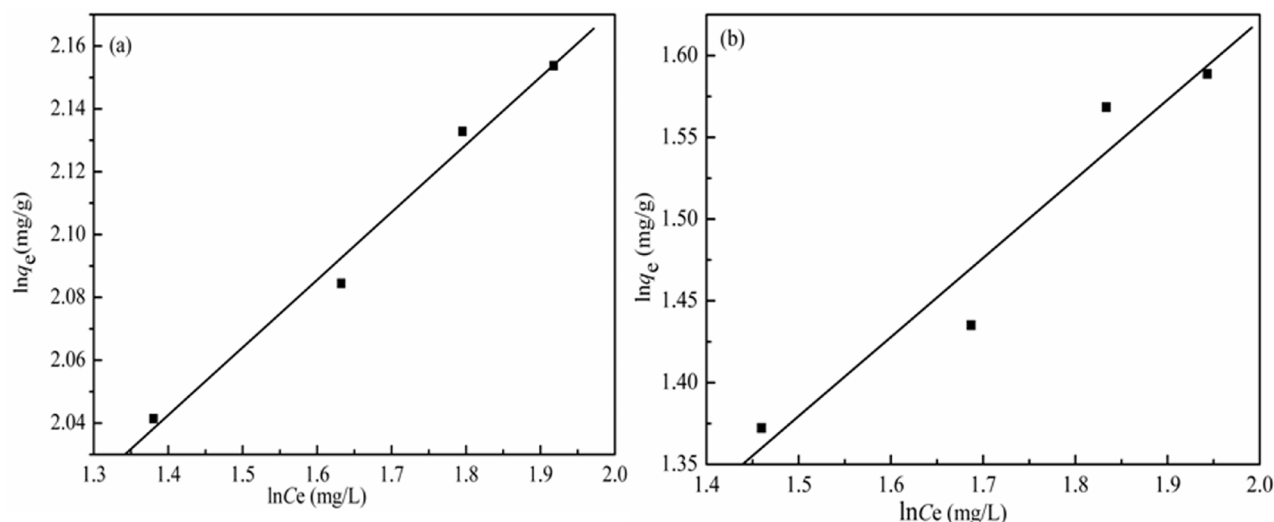


Fig. 9. Fitting results of Freundlich model for Pb^{2+} (a) and phenol (b) adsorption.

Table 2
Fitting parameters of Langmuir and Freundlich isotherm models

Adsorbate	Langmuir isotherm model			Freundlich isotherm model		
	q_m (mg/g)	b (L/mg)	R^2	K_f (mmol $^{1-n}$ L n /kg)	n	R^2
Pb^{2+}	131.6	0.27	0.989	55.12	4.65	0.993
Phenol	90.74	0.01	0.876	2.99	2.07	0.966

isotherm model is shown in Fig. 9. The parameters of the fitting result are listed in Table 2. According to the correlation coefficient R^2 in Table 2, the adsorption process of $\text{NH}_2\text{-SH-GO/o-MWCNTs}$ for Pb^{2+} and phenol conformed to the Freundlich isotherm model. By taking the adsorption process for phenol as an example, the correlation coefficients of Langmuir and Freundlich models were 0.876 and 0.966, respectively. Therefore, the adsorption process of $\text{NH}_2\text{-SH-GO/o-MWCNTs}$ for Pb^{2+} and phenol conformed to the Freundlich isotherm model as evinced by the correlation coefficient. This meant that phenol interacted with itself and the adsorbates, thus being a multilayer adsorption process, as was the case for the adsorption of lead ions. Additionally, the adsorption process occurred readily as the adsorption intensity constant n was within the range from 2 to 10. The adsorption intensity constant of Pb^{2+} ranged from 2 to 10 while that of phenol was around 2, which implied that the adsorption reaction of the adsorbent for Pb^{2+} and phenol occurred readily. Moreover, the value of K_f for Pb^{2+} during the adsorption process was larger than that for phenol. And the former was about 18 times that of the latter, implying that Pb^{2+} was more easily adsorbed using the adsorbent so that the adsorption capacity for Pb^{2+} was larger than that for phenol [36].

4. Conclusion

This study investigated the scale-inhibition effect and influence of different initial concentrations on the adsorption process for Pb^{2+} and phenol in circulating water under

the synergistic effect of a magnetic field and $\text{NH}_2\text{-SH-GO/o-MWCNTs}$. The $\text{NH}_2\text{-SH-GO/o-MWCNTs}$ were first prepared, and then characterized by using TEM and FT-IR. Additionally, changes in pH, conductivity, molecular activation energy, relative variations of intramolecular energy and the proportion of free water and adsorption capacity of the adsorbent were studied under different initial concentrations. TEM images suggested that GO was connected with MWCNTs where the MWCNTs were 30–40 nm in diameter while GO had a thin, sheet-like structure. With increased initial concentrations, the molecular activation energies of circulating water grew while intramolecular energy did not undergo significant change. Moreover, the relative variation of the proportion of free water rose as well as the equilibrium adsorption capacities for Pb^{2+} and phenol. The equilibrium adsorption capacities for Pb^{2+} and phenol separately reached 142.42 mg/g and 48.34 mg/L at an initial concentration of 90 mg/L. The adsorption process for Pb^{2+} and phenol conformed to the pseudo-second-order kinetic model and Freundlich isotherm model under the synergistic effect of a magnetic field and $\text{NH}_2\text{-SH-GO/MWCNTs}$.

Acknowledgement

The authors are grateful for the financial support received from The National Natural Science Foundation of China (51304101, 51764039), Youth Science and Technology Fund Project of Gansu Province (1606RJYA305, 17JR5RA116) and Doctor Research Cost of Lanzhou University of Technology (061702).

References

- [1] P.F. Wang, M.H. Cao, C. Wang, Kinetics and thermodynamics of adsorption of methylene blue by a magnetic graphene-carbon nanotube composite, *Appl. Surf. Sci.*, 290 (2014) 116–124.
- [2] M.A. Barakat, New trends in removing heavy metals from industrial wastewater, *Arab. J. Chem.*, 4 (2011) 361–377.
- [3] L.F. Chen, H.W. Liang, Y. Lu, C.H. Cui, S.H. Yu, Synthesis of an attapulgite clay@carbon nanocomposite adsorbent by a hydrothermal carbonization process and their application in the removal of toxic metal ions from water, *Langmuir*, 27 (2011) 8998–9004.
- [4] L.L. Jiang, H.T. Yu, X.M. Zhou, X.G. Hou, Z.S. Zou, S.J. Li, C.T. Li, X.Y. Yao, Preparation, characterization, and adsorption properties of magnetic multi-walled carbon nanotubes for simultaneous removal of lead(II) and zinc(II) from aqueous solutions, *Desal. Wat. Treat.*, 57 (2016) 18446–18462.
- [5] L.H. Ai, J. Jiang, Removal of methylene blue from aqueous solution with self-assemble cylindrical graphene-carbon nanotube hybrid, *Chem. Eng. J.*, 192 (2012) 156–163.
- [6] Y. Zhang, C. Chu, T. Li, S. Xu, L. Liu, M. Ju, A water quality management strategy for regionally protected water through health risk assessment and spatial distribution of heavy metal pollution in 3 marine reserves, *Sci. Total Environ.*, 599 (2017) 721–731.
- [7] A.N. Deva, C. Arun, G. Arthanareeswaran, P. Sivashanmugam, Extraction of peroxidase from waste *Brassica oleracea* used for the treatment of aqueous phenol in synthetic wastewater, *J. Environ. Chem. Eng.*, 2 (2014) 1148–1154.
- [8] P. Muchez, M. Corbella, Factors controlling the precipitation of copper and cobalt minerals in sediment-hosted ore deposits: advances and restrictions, *J. Geochem. Explor.*, 118 (2012) 38–46.
- [9] C.T. Li, S.L. Zhu, Research on phenol wastewater treatment by electrochemical oxidation, *Electrochemistry*, 11 (2005) 101–103.
- [10] Z.J. Dong, J.J. Yan, H.B. Tu, Studying on the preparation and application of silica aerogel composites for thermal insulation, *New Chem. Mater.*, 33 (2005) 46–48.
- [11] X.H. Zhang, H.L. Zhao, F. He, Preparation and surface modification of SiO₂ aerogel by ambient pressure drying, *J. Univ. Sci. Technol. B.*, 28 (2006) 157–162.
- [12] Y.M. Chen, K. Xie, D.F. Zhao, Preparation and hydrophobic modification of SiO₂ aerogels, *Aerosp. Mater. Technol.*, 1 (2006) 30–33.
- [13] V.K. Gupta, I. Ali, T.A. Saleh, A. Nayak, S. Agarwal, Chemical treatment technologies for wastewater recycling-an overview, *RSC Adv.*, 2 (2012) 6380–6388.
- [14] L.L. Jiang, X.Y. Yao, H.T. Yu, X.G. Hou, Z.S. Zou, F.M. Shen, C.T. Li, Effect of permanent magnetic field on water association in circulating water, *Desal. Wat. Treat.*, 79 (2017) 152–160.
- [15] Lili Jiang, Shujun Li, Haitao Yu, Zongshu Zou, Xingang Hou, Fengman Shen, Chuantong Li, Xiayan Yao, Amino and thiol modified magnetic multi-walled carbon nanotubes for the simultaneous removal of lead, zinc, and phenol from aqueous solutions, *Appl. Surf. Sci.*, 369 (2016) 398–413.
- [16] Y. Shen, Q. Fang, B. Chen, Environmental applications of three-dimensional graphene-based macrostructures: adsorption, transformation, and detection, *Environ. Sci. Technol.*, 49 (2015) 67–84.
- [17] S. Iijima, Helical microtubules of graphitic carbon, *Nature*, 354 (1991) 56.
- [18] Y. Tian, B. Gao, V.L. Morales, Methods of using carbon nanotubes as filter media to remove aqueous heavy metals, *Chem. Eng. J.*, 210 (2012) 557–563.
- [19] Z.W. Xu, Y.Y. Zhang, X.M. Qian, J. Shi, L. Chen, B.D. Li, J.R. Niu, L.S. Liu, One step synthesis of polyacrylamide functionalized graphene and its application in Pb(II) removal, *Appl. Surf. Sci.* 316 (2014) 308–314.
- [20] L.L. Jiang, C.T. Li, H.T. Yu, Z.S. Zou, F.M. Shen, X.G. Hou, Preparation of NH₂-SH-GO/MWCNTs composite for simultaneous removal of Pb(II), Zn(II) and phenol from aqueous solution, *Desal. Wat. Treat.*, 97 (2017) 272–284.
- [21] H. Alijani, Z. Shariatinia, A.A. Mashhadi, Water assisted synthesis of MWCNTs Over natural magnetic rock: an effective magnetic adsorbent with enhanced mercury(II) adsorption property, *Chem. Eng. J.*, 281 (2015) 468–481.
- [22] H.B. Wang, W. Wang, Y.F. Zhao, Z.W. Xu, L. Chen, L.H. Zhao, X. Tian, W.Y. Sun, Superior adsorption of 3D nanoporous architectures for Ni(II) ions adsorption using polyvinyl alcohol as cross-linking agent and adsorption conveyor, *RSC Adv.*, 8 (2018) 7899–7903.
- [23] H. Al-Gohani, M.A. Salam, Kinetics and thermodynamics study of aniline adsorption by multiwalled carbon nanotubes from aqueous solution, *J. Colloid Interf. Sci.*, 360 (2011) 760–767.
- [24] G.E. Cunningham, A new interpretation of the adsorption isotherm, *J. Phys. Chem.*, 39 (1934) 69–77.
- [25] L. Zhou, S. Pan, X. Chen, Kinetics and thermodynamics studies of pentachlorophenol adsorption on covalently functionalized Fe₃O₄@SiO₂-MWCNTs core-shell magnetic microspheres, *Chem. Eng. J.*, 257 (2014) 10–19.
- [26] H. Hosoda, H. Mori, N. Sogoshi, Refractive indices of water and aqueous electrolyte solutions under high magnetic fields, *J. Phys. Chem.*, 108 (2004) 1461–1464.
- [27] Y.H. Yuan, L.Y. Cai, T.L. Yue, Z.P. Gao, X.B. Zhao, Kinetics and thermodynamics analysis of apple polyphenols adsorption by aminated magnetic chitosan microspheres, *Trans. Chin. Soc. Agr. Eng.*, 28 (2012) 264–269.
- [28] Z.C. Miao, F. Wang, D. Deng, Thermodynamics of phenol adsorption on the microsphere based on starch, *Adv. Mater. Res.*, 550 (2012) 2629–2632.
- [29] H. Chen, J. Li, D. Shao, Poly (acrylic acid) grafted multiwall carbon nanotubes by plasma techniques for Co (II) removal from aqueous solution, *Chem. Eng. J.*, 210 (2012) 475–481.
- [30] F. Wang, Y. Wang, Y. Li, Preparation of 6-diallylamino-1, 3, 5-triazine-2, 4-disulfidryl functional nanofilm by electrochemical polymerization technique on aluminum surface, *Int. J. Electrochem. Sci.*, 6 (2011) 793–803.
- [31] C.C. Liu, Y.S. Li, Y.M. Chen, Removal of methylene blue from aqueous solution using wine-processing waste sludge, *Water Sci. Technol.*, 65 (2012) 2191–2199.
- [32] M. Hadavifar, N. Bahramifar, H. Younesi, Adsorption of mercury ions from synthetic and real wastewater aqueous solution by functionalized multi-walled carbon nanotube with both amino and sulfhydrylated groups, *Chem. Eng. J.*, 237 (2014) 217–228.
- [33] H. Al-Johani, M.A. Salam, Kinetics and thermodynamic study of aniline adsorption by multi-walled carbon nanotubes from aqueous solution, *J. Colloid Interface Sci.*, 360 (2011) 760–767.
- [34] O. Olanipekun, A. Oyefusi, G.M. Neelgund, A. Oki, Adsorption of lead overgraphite oxide, *Spectrochim. Acta Part a-Mol. Biomol. Spectrosc.*, 118 (2014) 857–860.
- [35] L. Fan, C. Luo, M. Sun, X. Li, H. Qiu, Highly selective adsorption of lead ions by water-dispersible magnetic chitosan/graphene oxide composites, *Colloids Surf. B: Biointerface*, 103 (2013) 523–529.
- [36] R. Fu, Y. Liu, Z. Lou, Adsorptive removal of Pb (II) by magnetic activated carbon incorporated with amino groups from aqueous solutions, *J. Taiwan Inst. Chem. Eng.*, 62 (2016) 247–258.